communications earth & environment

Article

A Nature Portfolio journal

https://doi.org/10.1038/s43247-026-03785-5

Targeted adaptation options can effectively reduce amplified compound water-heat stress around maize flowering in China

Check for updates

Mingxia Huang [1,2], Jing Wang [1,3] ✉, Bin Wang [4,5,6] ✉, Christoph Müller [7], Jonas Jägermeyr[7,8,9], De Li Liu [4,6,10], Hong Yin[2], Bo Lu [2], Keyu Xiang[4,11] & Senthold Asseng [12]

Compound water and heat stresses cause great crop yield losses, threatening food security. However, the current extent and future trajectory of these stresses remain uncertain. Here, we developed a compound water-heat stress index (WHSI) to quantify the spatiotemporal variations in co-occurring water and heat stresses around maize flowering in China. We demonstrated that WHSI can effectively capture historical yield variations in major maize-growing regions. Future projections show a substantial increase in compound water-heat stress events, particularly in northeast and northwest of China, driven primarily by rising temperature. By optimizing planting dates and selecting suitable cultivars, compound water-heat stress can be alleviated by more than 70% through dynamic adaptation (site- and year-specific adjustments), representing a potential upper bound of adaptation under the strategies considered. These results highlight the critical role of targeted adaptation measures implemented to mitigate the worsening impact of amplified compound water-heat stress on crop yield.

The soaring global population and shrinking world's cropland area pose immense pressure on grain production[1,2]. Doubling the production of global major cereal crops is required to feed over 9.7 billion people by 2050[3]. Given the limited availability of arable land, achieving a consistently high yield per hectare becomes crucial in combating potential food crises[4]. However, the escalating frequency of extreme weather and climate events due to climate change, such as droughts and heatwaves, poses a great threat to crop yield[5,6]. Climate change presents a substantial challenge for global food security, especially with respect to the stability of global food systems.

Maize holds a prominent position as a staple grain and feed crop, with the highest global production levels[7,8]. In 2021, global maize production reached 1.21 billion metric tons, while maize production in China accounted for approximately 18.4% of the global total[8]. China's maize cultivation spans across a wide range of latitudes (23–48°N) with contrasting climate conditions. During the maize growing seasons, the southwest planting regions exhibited substantially higher temperatures from 1980 to 2009, with mean seasonal values approximately 6 °C warmer than those in northeastern China, and received nearly 500 mm more precipitation compared to northwestern regions[9]. Future climate projections suggest amplified spatial heterogeneity in temperature changes, particularly stronger warming trends in high-latitude maize cultivation areas[10]. Concurrently, the combined effects of intensified evapotranspiration and reduced precipitation are projected to exacerbate aridity in central and eastern China, whereas western regions may experience a wetting trend under climate change scenarios[11]. In addition, China frequently encounters various agro-meteorological disasters that cause significant losses in maize yield. For

[1]College of Resources and Environmental Sciences, China Agricultural University, Beijing, China. [2]National Climate Center, China Meteorological Administration, Beijing, China. [3]CMA-CAU Joint Laboratory of Agriculture Addressing Climate Change, Beijing, China. [4]NSW Department of Primary Industries, Wagga Wagga Agricultural Institute, Wagga Wagga, NSW, Australia. [5]Hawkesbury Institute for the Environment, Western Sydney University, Richmond, NSW, Australia. [6]Gulbali Institute for Agriculture, Water and Environment, Charles Sturt University, Wagga Wagga, NSW, Australia. [7]Member of the Leibniz Association, Potsdam Institute for Climate Impacts Research (PIK), Potsdam, Germany. [8]NASA Goddard Institute for Space Studies, New York, NY, USA. [9]Climate School, Columbia University, New York, NY, USA. [10]Climate Change Research Centre, University of New South Wales, Sydney, NSW, Australia. [11]School of Life Sciences, Faculty of Science, University of Technology Sydney, Sydney, NSW, Australia. [12]Department of Life Science Engineering, Digital Agriculture, HEF World Agricultural Systems Center, Technical University of Munich, Freising, Germany. ✉e-mail: wangj@cau.edu.cn; bin.a.wang@dpi.nsw.gov.au

example, maize cultivation in the North China Plain is frequently affected by extremely high temperatures during the flowering stage, while fluctuations in precipitation greatly impact maize production in northeast China[12,13].

Extreme water and heat stresses can hamper maize growth and development as well as grain formation and ultimately result in productivity losses[14,15]. Recent studies have highlighted substantial crop yield reductions attributed to compound water and heat stresses globally, affecting important maize production regions such as the USA, Australia, Europe, Brazil, and China[16–19]. Compound water-heat stress occurs when water and heat stresses coincide due to their physical interdependency in the climate system[20]. Notably, the 2003 heatwave, accompanied by drought in France, resulted in national yield losses of approximately 17.6% compared to the average between 2000 and 2006[21,22]. Extreme weather and climate events are projected to increase in frequency and intensity in the future, particularly increasing water and heat stresses[23,24]. Additionally, due to the enhancing effect of high temperature on drought[25], compound heat and water stresses face a higher risk of occurrence in the future[20]. It is projected that the global land area affected by compound drought and heat events will increase by almost 70–80% by the end of the 21st century under the Representative Concentration Pathway 8.5[26].

Previous studies have developed various indices representing compound water and heat stresses based on precipitation and temperature, often overlooking the water and heat limitations for crop growth and development[27–29]. Specifically, drought damage to crops depends on the supply of soil water availability to crop transpiration, making precipitation a less accurate proxy of root-accessible soil moisture. For heat damage, high temperature thresholds were often set as a constant during the maize growth period; however, field experiments showed that high temperature thresholds varied with the phenological stages. This hinders the applicability of the current compound water-heat stress index in accurately evaluating the impacts of compound water and heat stresses on crop production[23]. Therefore, it is necessary to develop an index that can track the combined stress on crop growth. To address this issue, we applied a process-based crop model (APSIM 7.7) to simulate crop phenology and soil water dynamics by taking into account the interactions between cultivars, environment, and management[30,31]. However, most crop models, including APSIM, underestimate the impact of heat stress on maize growth and yield[32]. Therefore, we calculated heat stress based on cumulative daily maximum temperatures above phenological stage-specific optimal temperature thresholds for maize. The compound water-heat stress index was then developed based on the co-occurrence of water and heat stress events by considering their distribution[20].

While combined water and heat stresses have detrimental effects on crop growth and development throughout the entire growth period, their impact varies with the phenological stages of the crop[33]. Notably, stresses around flowering, a critical period for maize pollination and grain formation, result in more adverse impacts by decreasing grain set and size than those occurring during other growth stages[34–36]. Therefore, alleviating the compound water and heat stresses around flowering is a priority in adapting to future climate change[32]. Adjusting planting dates and selecting suitable cultivars have been recognized as the most effective adaptation options in tackling climate change by altering the flowering date to avoid compound water and heat stresses[9,37]. Recent studies have shown that optimizing planting dates and cultivars could help alleviate 50% and 29% of maize yield losses caused by extreme temperature events in Iran and the North China Plain, respectively, during 2040–2070[9,38].

Developing and implementing targeted adaptation strategies would assist farmers in using suitable planting dates and cultivars with different growth cycles to reduce the impacts of extreme weather and climate events under climate change[39,40]. However, implementing different adaptation strategies over different time frames can result in high adaptation costs. For example, employing a particular set of adaptation measures for each location and each year may provide a greater adaptation capacity, but may incur higher adaptation costs and require accurate climate prediction information for upcoming years compared to implementing the identical adaptation strategy across multiple years. The adaptation costs mainly include customizing management practices, breeding and selecting cultivars with appropriate maturity types, and generating high-resolution weather forecasts and climate predictions[41,42]. Assessing the adaptation potential of different adaptation strategies is crucial for breeders, policymakers, and local growers, as it provides valuable insights for identifying the most effective agronomic management options to safeguard grain production.

However, current assessments face critical limitations in three key aspects. First, predominant stress indices focus solely on event frequency while neglecting the concurrent intensity and temporal clustering of compound water-heat stress during key growth stages for crops. Second, quantitative evaluations of adaptation strategies remain insufficient, particularly their capacity to reduce climate risks under varying climate scenarios. Third, the comparative efficacy of static site-specific adaptations versus dynamic forecast-responsive strategies to mitigate compound stress has not been conducted in climate change impact assessment. To address these knowledge gaps, here we focused on China's Maize Belt to (1) develop a combined water-heat stress index (WHSI) to quantify compound water and heat stresses around flowering, (2) quantify the impacts of climate change on the frequency and intensity of combined water-heat stress, and (3) assess the adaptation capacity of different adaptations in combating compound water-heat stress during flowering.

Results

Compound water-heat stress index

To quantify the intensity and frequency of compound water-heat stress, we devised a water-heat stress index (WHSI) by integrating the individual water stress index (WSI) and heat stress index (HSI) of compound events. The WSI was defined as the cumulative daily water deficit, expressed as one minus the ratio of actual to potential evapotranspiration, normalized by the total window of maize flowering period. The HSI was calculated as the cumulative exceedance of daily maximum temperature above a defined threshold, relative to a lethal temperature limit, also normalized by the flowering window. The intensity and frequency of high temperature and drought stress occurrence were respectively integrated into the WSI and HSI indices through a cumulative process. The data structures of WSI and HSI are illustrated in Fig. 1b, c. Compound stress events were identified as periods when both water and heat stresses occurred concurrently for three or more consecutive days (Fig. 1a). The WHSI was then computed using a joint probability distribution of WSI and HSI during these compound events, capturing their interdependence and the compound nature of the stresses. A higher WHSI value indicates more intense compound stress, reflecting severe and simultaneous water and heat impacts (Fig. 1d).

To evaluate the impact of WHSI on maize yield, we used the Spearman's correlation coefficient (r) to measure the correlation of WHSI with de-trended maize yield in each province where compound stress around flowering occurred during the historical period (Supplementary Note 1, Supplementary Fig. 1). The de-trended yield isolates the climate-driven component of maize yield by removing non-climatic trends (e.g., technological advancements). To model these trends, we applied both linear regression and second-order polynomial regression (Supplementary Note 2). The better-fitting model (selected based on R^2) was retained to predict the technological trend. The de-trended yield was then calculated as the residual between observed yield and the model-predicted trend. We investigated the capability of WHSI in capturing low yields in extreme years using 38 years of maize yield data (1980–2017) from major maize-producing provinces. In order to focus on the effects of compound water-heat stress on maize yields, we calculated r between WHSI and de-trended yield based on the years with minimal climatic stress, i.e., considering only those with a cumulative probability of de-trended maize yields above 80%, as well as years with high compound water-heat stress, identified by a cumulative probability of WHSI above 80% (Fig. 2a, b). Note that the thresholds for WHSI and de-trended yield exceeding 80% varied with regions (Supplementary Fig. 2). Figure 2c–i depicts the relationship between WHSI around maize flowering and de-trended maize

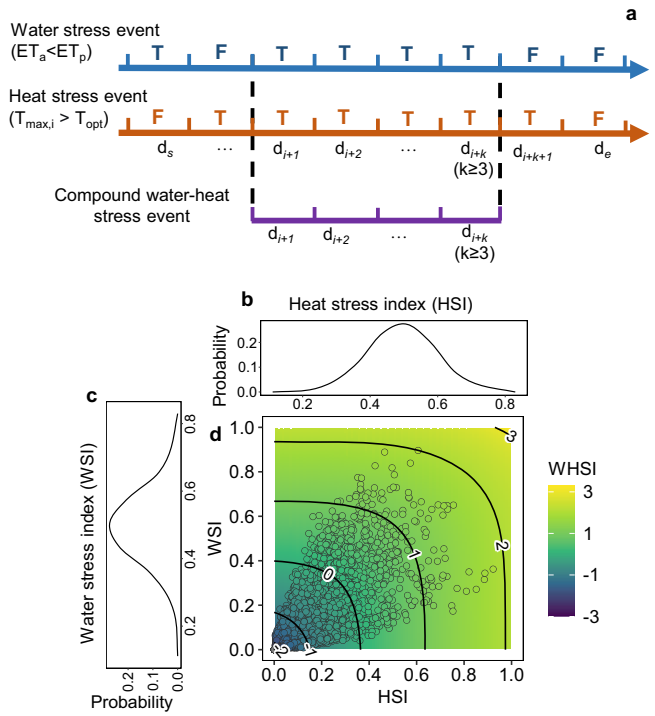


Fig. 1 | Diagram of relationship between water stress, heat stress, and compound water-heat stress events. a Definition of water stress, heat stress, and compound stress. T (True) indicates the occurrence of stress, while F (False) indicates the absence of stress. ET_a and ET_p are the daily actual and potential evapotranspiration, respectively. $T_{max,i}$ is the maximum air temperature of the *i*th day during the flowering period, while T_{opt} is the physiological optimal temperature for maize specific growth period. d_s, d_e, and d_i represent the start date, end date, and any date of the flowering period. *k* is the length of a compound stress event. **b**–**d** are illustrative examples showing the probability distribution of HSI and WSI as well as the value of WHSI. Dots **d** represent observed compound stress conditions derived from maize-growing regions in China during 1980–2018, illustrating the relationship among HSI, WSI, and WHSI under real-world conditions. Higher WSI and HSI values indicate more severe water and heat stresses, respectively, while higher WHSI indicates greater severity of compound water–heat stress.

yield in staple maize planting provinces that suffered extreme compound water-heat stress during 1980–2017. The negative values of *r* (WHSI, de-trended yield) in all provinces indicated that higher WHSI resulted in higher yield loss.

To rigorously evaluate the robustness of the WHSI, we conducted a sensitivity analysis by varying key parameters, including the duration of compound events, the definition of the flowering window, and the temperature thresholds used in the HSI. The selected parameter combinations showed significant correlations with observed de-trended maize yields and were also supported by physiological understanding from the literature (Supplementary Note 3, Supplementary Fig. 3, Supplementary Tables 1–3). We further validated the WHSI using de-trended yield data from agro-meteorological stations (Supplementary Fig. 4a), where the Spearman's correlation coefficient (*r*) ranged from −0.6 to −0.5 (Supplementary Fig. 5), indicating a significantly negative relationship between WHSI and yield. In addition, the Nash–Sutcliffe efficiency (NSE) for the relationship between WHSI-predicted yield losses and observed de-trended yield losses exceeded 0.5 in most provinces, suggesting a satisfactory level of predictive performance (Supplementary Fig. 6). To further assess the capability of WHSI in capturing extreme events, we compared its spatial patterns between an observed severe drought year (1997) and a normal year (1995) in Northwest China and the North China Plain. The WHSI values were substantially higher during the severe drought year, corresponding to larger observed de-trended yield losses (Supplementary Fig. 7). Based on these validations, WHSI was subsequently employed as a quantitative metric for assessing compound water–heat stress severity in the following analyses.

The spatial-temporal evolution of WHSI

Based on the constructed compound water-heat stress index, we evaluated the spatial-temporal evolution characteristics of WHSI. Figure 3a illustrates the spatial variations of WHSI over China's maize planting regions during four time periods. For studying the future, simulations were conducted using five selected Global Climate Models (GCMs, Supplementary Table 4) under the Shared Socio-Economic pathways 2–4.5 and 5–8.5 (SSP2–4.5 and SSP5–8.5), respectively, capturing possible changes in temperature and precipitation (see "Material and methods"). The analysis was conducted across 277 meteorological sites within China's Maize Belt.

The threshold value of −3.1 corresponds to negligible HSI and WSI values (approaching zero), indicating minimal compound stress. Therefore, WHSI values exceeding −3.1 are assumed to be detrimental to maize. We found that in total 76% of the study sites suffered at least one year of compound water-heat stress (WHSI > −3.1) during the maize flowering period over the baseline period (1980–2009), with consistent results under both SSP2–4.5 and SSP5–8.5 (Fig. 3a, Supplementary Fig. 8). Compared to the baseline, the number of sites affected by these stresses would increase by 9.2%, 9.6%, and 13.2% in the 2020s, 2050s, and 2080s under SSP5–8.5, respectively. For the entire China's Maize Belt, the average WHSI values were projected to increase by 0.1, 0.4, and 0.5 in the 2020s, 2050s, and 2080s under SSP5–8.5, respectively, compared with the baseline (Fig. 3a). Under SSP5–8.5, Region I (Northeast China) and region II consistently demonstrated higher levels of compound stress under the future scenarios compared to other three regions. However, the compound stress in these regions showed larger differences between GCMs, especially in the 2050 s and 2080 s. In addition, region II was projected to experience a more severe increase of compound stress than the other four regions by four of five GCMs (Supplementary Table 5). Under SSP2–4.5, the spatial patterns of WHSI remained consistent with those under SSP5–8.5, while the magnitude of WHSI changes was smaller (Supplementary Fig. 8, Supplementary Table 6).

To clarify compound stress severity, the WHSI was categorized into mild, moderate, severe, and extreme levels using cumulative probabilities at the 75th, 50th, and 25th percentiles. The same threshold classification was applied across all regions to ensure comparability of compound stress severity among different maize-growing regions. As shown in Fig. 2, severe and extreme compound stresses (WHSI > −0.4, Fig. 3b) resulted in heavy yield reductions. The occurrence frequency of each level was quantified by the cumulative years (Fig. 3b), which provides an empirical estimate of the probability of exceeding the corresponding WHSI thresholds. During the baseline, for extreme compound stress, region II (Northwest China) and region III (the North China Plain) exhibited relatively high occurrence frequencies, reaching 11.8% and 16.1%, respectively (Fig. 3d). Compared to the baseline, extreme compound stresses in all regions were projected to increase in the 2020s, 2050s, and 2080s except in region III. Notably, extreme compound stress was projected to increase by 17.7% in region I and 37.3% in region II in the 2080s (Fig. 3d). Under SSP2–4.5, the projected changes in all levels of compound stress showed similar trends to those under SSP5–8.5 (Fig. 3c).

To illustrate the relative contribution of change in water stress and heat stress to the overall change in WHSI, we explored the spatial and temporal changes of individual water and heat stress (Fig. 4). The WSI and HSI, ranging from 0 to 1, were used to assess water and heat stresses. Both indices indicate harmful conditions when their values exceed 0, with higher values representing greater stress. During 1980–2100, water stress around maize flowering was more severe in regions I and II than in other regions. With the progression of climate change, the projected mean WSI from all GCMs indicated minimal changes across all regions. The trend of WSI changes exhibited a larger variance across all GCMs in all regions under both SSP5–8.5 and SSP2–4.5 (Supplementary Tables 7 and 8), indicating high projection uncertainty despite limited absolute changes. In contrast,

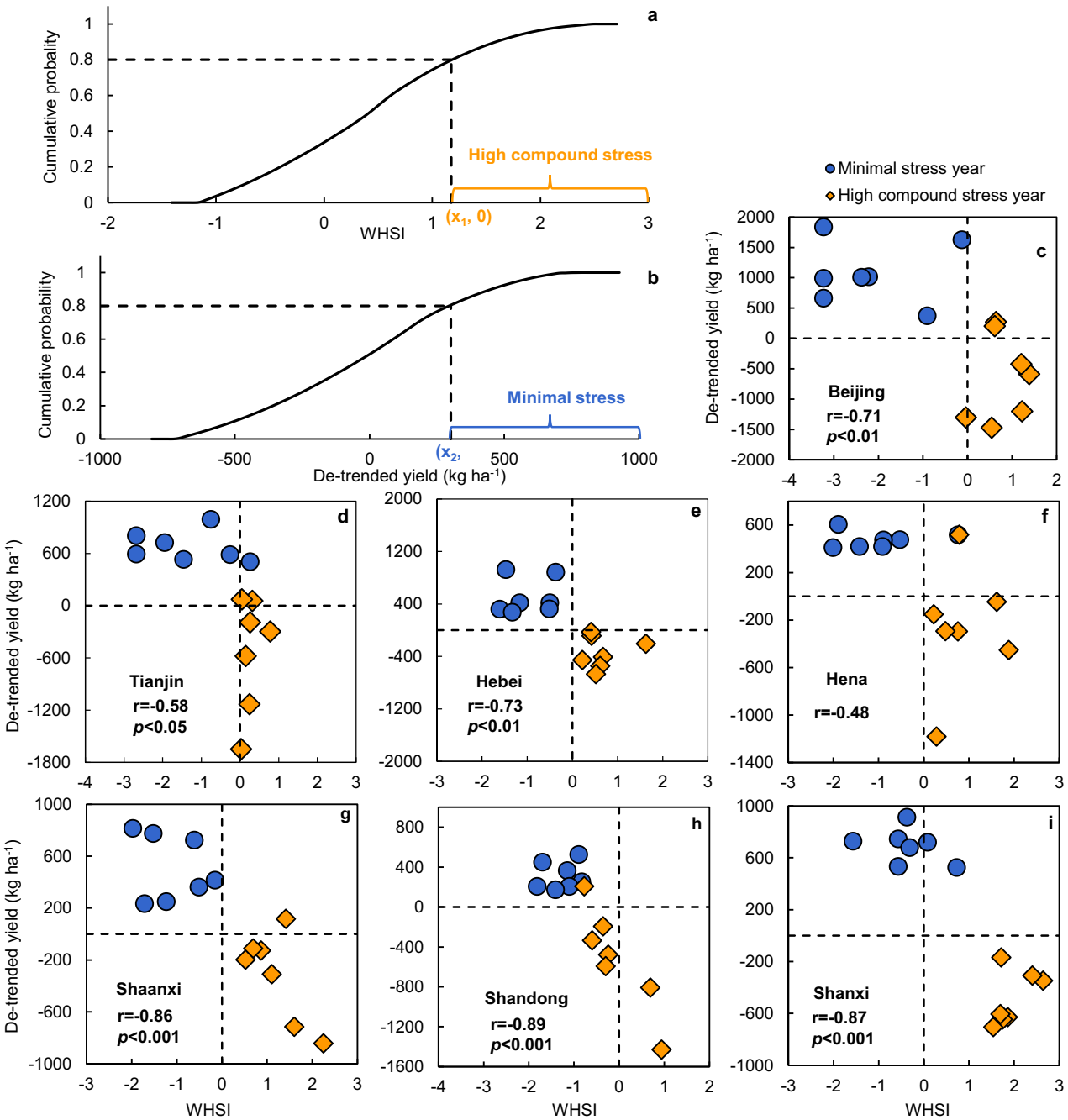


Fig. 2 | Correlation between the compound water-heat stress index (WHSI) and province-level maize yield. a, **b** Probability distribution of WHSI and de-trended maize yield. **c–i** Correlation between WHSI and de-trended yield under minimal stress years and high water-heat compound stress years in major maize planting provinces. The minimal stress year is defined as the year in which the cumulative probability of de-trended maize yields exceeds 80%. The high compound stress year is defined as the year in which the cumulative probability of WHSI exceeds 80%. Supplementary Fig. 2 depicts the thresholds for WHSI (x_1) and de-trended yield (x_2) exceeding 80% in each province.

projected heat stress from all the GCMs would significantly increase ($p < 0.01$) across all the regions under both SSP5–8.5 and SSP2–4.5 (Supplementary Tables 9 and 10). As a result, increasing heat stress was mainly responsible for the projected rise of compound water-heat stress.

Adaptation capacity to compound water-heat stress

Given intensified compound water-heat stress caused by climate change, we proposed the implementation of adaptation strategies focusing on shifting the flowering date through adjustments in planting date and cultivar. The planting dates were adjusted within the potential planting window, ensuring that maize could grow without the risk of autumn frost and without hindering the subsequent crop's growth (see "Materials and methods"). Cultivars were selected from existing cultivars with different maturity types. Two adaptation levels were evaluated to mitigate compound stress. The first is site-specific adaptation using one optimal planting date and cultivar for each site over the years, which is a feasible level of adaptation. The second is dynamic adaptation, tailoring the adaptation to each site and each year, which represents an ideal level of adaptation (Fig. 5).

To quantify the efficacy of each adaptation level, we assessed "adaptation capacity," which was defined as the proportion of compound stress reduction achieved through implemented measures relative to the corresponding period stress without adaptation across study sites. The metric was

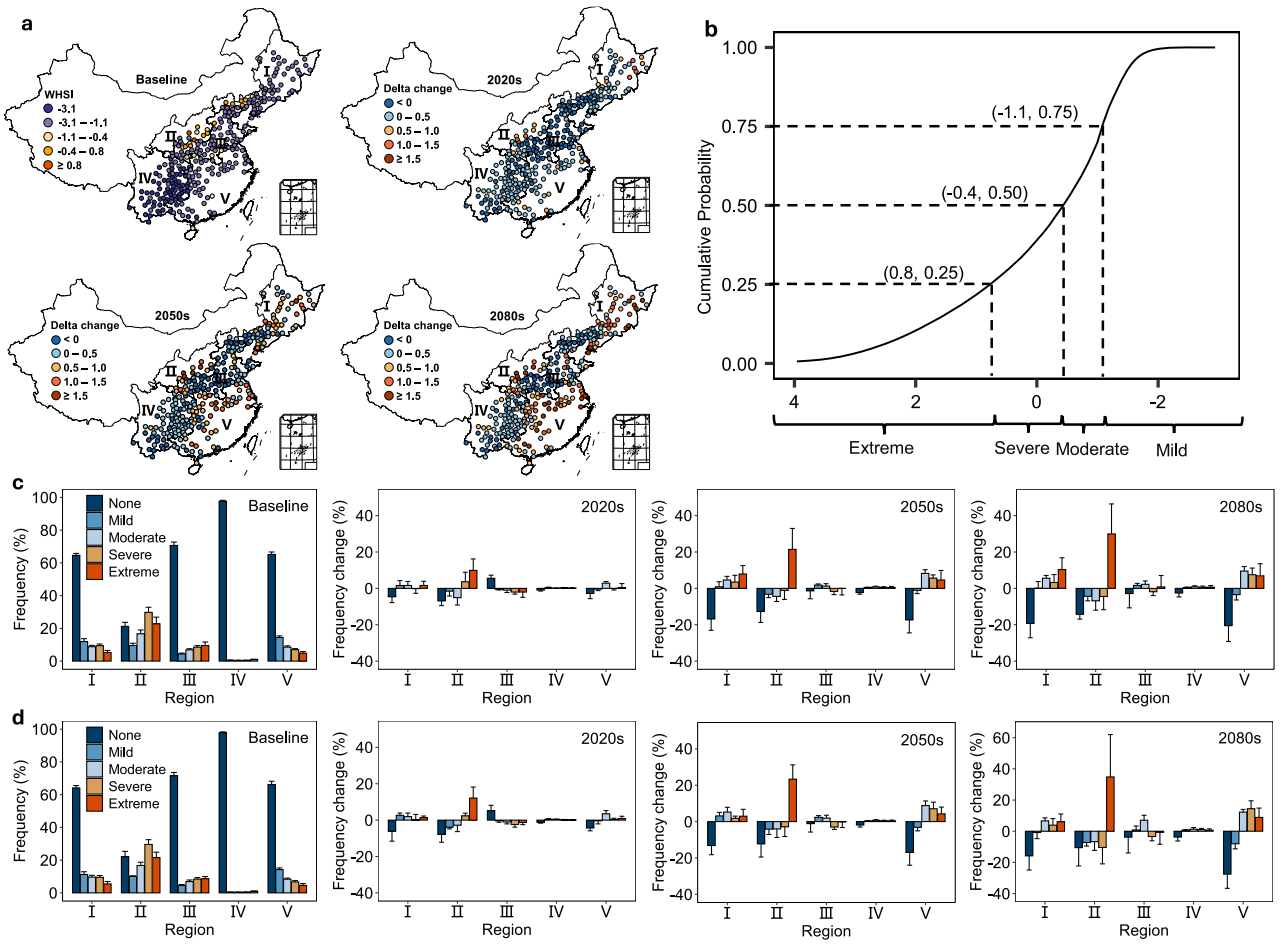


Fig. 3 | Impacts of climate change on the water-heat stress index (WHSI) around maize flowering in 1980–2099 in China's Maize Belt. a Spatial distribution of WHSI under the baseline (1980–2009), and the change rates in the 2020s (2010–2039), 2050s (2040–2069), and 2080s (2070–2099) compared to the baseline based on the projected average of five GCMs under SSP5–8.5. The delta change was calculated as the change in WHSI between the 2020s, 2050s, and 2080s and the baseline at each site. **b** Compound stress levels classified based on the cumulative probability distribution of compound water and heat stress index (WHSI) across all sites, years, and GCMs. **c**, **d** Occurrence frequency of mild, moderate, severe, and extreme compound stress under the baseline (1980–2009), and changes in occurrence frequency of different levels of compound stress in the 2020s, 2050s, and 2080s compared with baseline under SSP2–4.5 (**c**) and SSP5–8.5 (**d**), respectively. Frequency was defined as the proportion of years experiencing each level of compound stress at each site, and provides an empirical estimate of the probability of exceeding the corresponding WHSI thresholds. The bars in panels **c** and **d** represent the average values across all sites and GCMs within each region, and error bars represent the SD of five GCMs. Regions I–V represent the Northeast China, the Northwest China, the North China Plain, the Southwest China, and the South China, respectively.

derived from changes in WHSI (Eq. 8). High adaptation capacity values (approaching 100%) indicated effective stress reduction, whereas low values (approaching 0) suggested persistent severe stress despite adaptation efforts. We conducted an assessment of the adaptation capacity of site-specific and dynamic adaptation strategies across China's Maize Belt (Fig. 6). The results indicate that dynamic adaptation has a greater capacity to mitigate compound stress, reducing it by an average of 70.6% and 74.3% across all regions during 1980–2099 under SSP5–8.5 and SSP2–4.5, respectively (Fig. 6a). In contrast, site-specific adaptation shows a lower mitigation capacity, with reductions of 52.9% and 54.9%, respectively (Fig. 6a). Furthermore, the adaptation capacity of both adaptation levels varied over the course of the simulation time period under both scenarios (Supplementary Fig. 9). Projected capacity of dynamic adaptation averaged across five GCMs would decrease with time in most regions under both scenarios, except for region III, indicating a potential increase in compound stress in the future even with adaptation. To further assess the sources of uncertainty, we quantified the uncertainty in adaptation capacity arising from multiple sources, including GCMs, SSPs, and adaptation levels. Across all regions, adaptation level was the dominant source of uncertainty, accounting for more than 40% of the total variance. Uncertainty associated with GCMs was the second largest contributor in all regions, with relatively higher contributions observed in regions III and IV (Supplementary Fig. 10).

We also compared the occurrence rates of optimal planting date and maturity type for all combinations of both adaptation levels under SSP5-8.5 (Supplementary Figs. 11–14). The results showed that early-maturing cultivars under early or late planting had higher adaptation capacity to compound stress for all regions, except for region II, where late-maturing cultivars under late planting had higher adaptation capacity to compound stress for both adaptation levels. Meanwhile, the combinations with higher adaptation capacity to compound stress for both adaptation levels were almost similar during different time periods (Supplementary Figs. 11 and 12). Under SSP2–4.5, the optimal combinations of cultivar maturity type and planting date were broadly similar to those identified under SSP5-8.5 (Supplementary Figs. 13 and 14).

The patterns of the frequency of different levels of compound stress with both adaptation strategies were broadly consistent, with a general shift from higher to lower stress categories across regions. Region II would experience the most reductions in extreme compound stress, with its frequency reduction of 17.8% and 11.1% under dynamic adaptation and site-specific adaptation under SSP5–8.5 (Fig. 6b). In regions IV and V, extreme

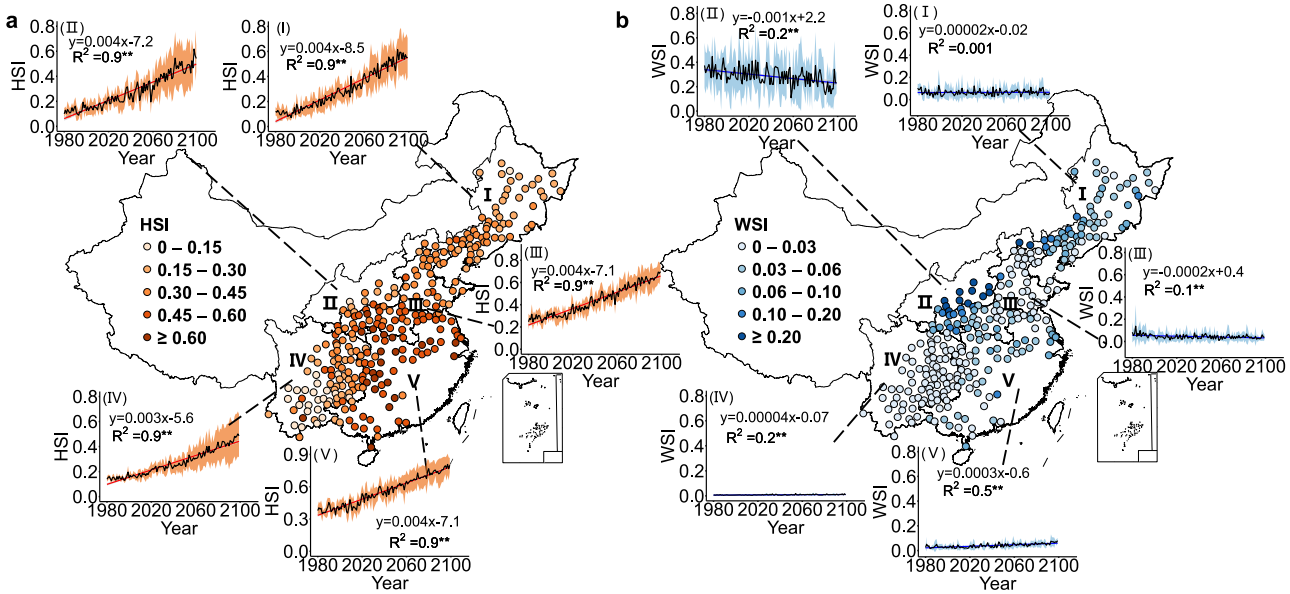


Fig. 4 | The distribution and temporal change of the heat stress index (HSI) and water stress index (WSI) around maize flowering in China's Maize Belt in 1980–2099 under SSP5–8.5. a and **b** represent HSI and WSI, respectively. The color points on the maps represent the average values of HSI and WSI during 1980–2099, and small line plots represent the changing trends of HSI and WSI in each planting region, and the gray shading represents the standard deviation of HSI and WSI based on five GCMs. $^{*}P < 0.05$, $^{**}P < 0.01$. The definitions of regions I–V are the same as in Fig.3.

stress frequency would decrease by 1.2% and 6.0% with dynamic adaptation, and 1.1% and 2.7% with site-specific adaptation under SSP5–8.5. Under SSP2–4.5, similar regional patterns in adaptation potential were observed between the two adaptation strategies, although the overall magnitude was slightly lower than that under SSP5–8.5 (Fig. 6b). For example, in region II, the frequency of extreme compound stress was projected to decrease by 17.1% and 11.1% with dynamic and site-specific adaptation, respectively, under SSP2–4.5 (Fig. 6b). Temporal analysis revealed consistent trends across different time periods. However, more severe and extreme compound stresses were projected to decrease over time under both adaptation strategies and scenarios (Supplementary Fig. 15).

Discussion

In this study, we introduced a combined water and heat stress index named WHSI to assess the spatial and temporal changes of compound water-heat stress around maize flowering in China's Maize Belt. WHSI differs from previous compound indices by considering additional crop-specific factors such as crop transpiration and root water uptake, estimated by a process-based crop model, and temperature thresholds for the pre-anthesis, anthesis, and early grain-filling stages of maize[43,44]. By considering these factors, WHSI captures the impact of compound water-heat stress on maize yield (Fig. 2), demonstrating its reliability as a monitoring and diagnostic index. The framework of the compound index developed in our study could be applied to other crops and regions to assess and project the impacts of current and future compound extreme weather and climate events on crop production.

Our analysis revealed a concerning trend of intensifying combined water-heat stress during the maize flowering period in the future in China. Specifically, we found an increase in the number of sites affected by compound stress in China's Maize Belt, with a projected increase over the next decades[45]. Previous studies have documented the escalation of compound meteorological drought and high temperature events in summer seasons worldwide[28,46]. We projected that Northeast China and Northwest China (regions I and II) would experience more severe compound stress in the future compared to other regions in China's maize belt. This is because these areas have suffered from combined water-heat stress[13], and would experience intensified heat stress, albeit slight alterations in water stress in the future (Fig. 4). Therefore, we inferred that the increase in compound water-heat stress during the maize flowering period was primarily attributed to the rising levels of heat stress. This aligns with previous studies, which found that heat events are major drivers of compound drought and heat stress in the summer[23,47,48]. Interestingly, despite the stronger increase in heat stress under SSP5–8.5, WHSI is not consistently higher than under SSP2–4.5. This is mainly because water stress does not increase significantly under SSP5–8.5 (Supplementary Fig. 16). This differs from projections based on meteorological drought indices across SSP scenarios[49], likely because our analysis focuses on the crop-specific flowering period, where precipitation variability and soil moisture constraints play a dominant role, and crop responses can limit the translation of increased temperature into water stress.

The increasing risk of compound water-heat stress on maize growth necessitates the development of planned adaptation strategies[39,40]. Adjusting the planting date and selecting appropriate cultivars with different maturity types have been identified as effective measures for adapting to climate change[9,50]. Our study revealed that altering the flowering date through adjustments in planting date and cultivar selection could alleviate compound stress across all regions. To explore the possible adaptation strategies to compound water-heat stress, we proposed an adaptation framework comprising site-specific adaptation and dynamic adaptation without and with considering interannual climate variation in the maize growing season, respectively (Fig. 5). In general, site-specific adaptation is a popular adaptation strategy used in published studies[42,51] because it can be easily implemented for a long period in the context of climate change. However, dynamic adaptation exhibited higher and more stable adaptation capacity compared with site-specific adaptation.

To distinguish between theoretical adaptation potential and practical farmer behavior, we compared historical shifts in observed planting dates from agro-meteorological stations with the optimal planting dates derived from dynamic adaptation (Supplementary Fig. 17). The results show that the optimal planting dates exhibit larger interannual variability and tend to occur slightly later than the observed planting dates. Specifically, farmers have gradually shifted toward later planting dates over recent decades, suggesting a clear tendency to adapt by moving closer to the theoretically optimal window. Although it needs to be supported by robust climate forecast information in each year and location[52], dynamic adaptation would be a pursuable goal with the development of climate prediction for sub-seasonal to seasonal and crop breeding innovations targeting climate

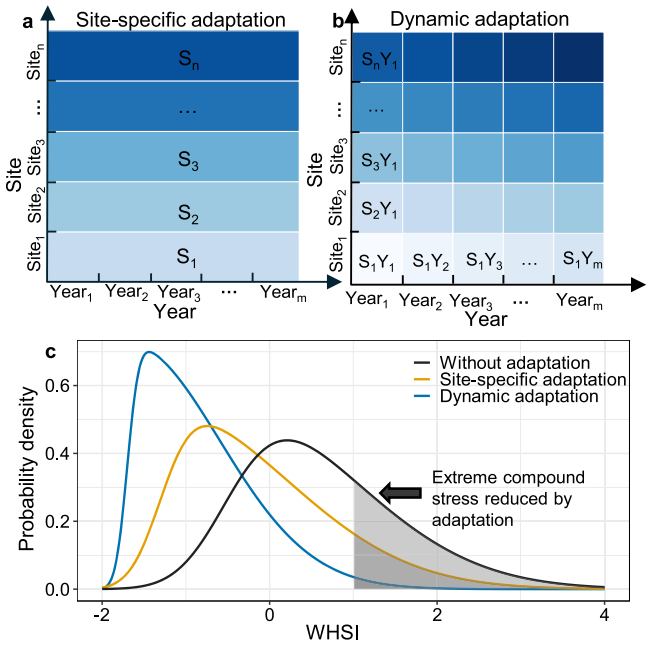


Fig. 5 | Schematic representation of different levels of adaptation to mitigate compound water-heat stress. a Different colors along the spatial scale (y-axis) indicate that each site has a fixed optimal adaptation scheme (sowing date and cultivar selection) across years. **b** Multiple colors with different intensities in the spatial (*y*-axis) and temporal (*x*-axis) scales represent each site, and each year has a set of optimal adaptation schemes. The symbols in grids represent the difference of optimal adaptation scheme in spatial scales by sites (Site 1, Site 2,…, Site *n*) and in temporal scale by years (Year 1, Year 2,…, Year *m*). **c** Schematic illustration of a probability density plot demonstrates how various adaptation strategies can effectively reduce the probability of extreme compound stress. The shaded area represents the probability of extreme compound stress (WHSI > 1).

resilience[53–55]. However, this scenario represents an idealized case assuming a high level of climate predictability and can be interpreted as an upper bound of adaptation potential rather than current farmer practice. Its practical implementation depends on further advances in climate forecasting and crop improvement. Encouragingly, emerging AI-driven approaches, such as deep learning-based climate models and hybrid physics-machine learning frameworks, are showing remarkable progress in improving both the precision and lead time of seasonal forecasts[56,57].

The considerable spatial heterogeneity in the adaptation capacity of different strategies emphasizes the importance of selecting adaptation approaches based on local weather and climate conditions. Region III suffered compound water-heat stress even with dynamic adaptation under baseline and 2020s (Supplementary Fig. 9). Previous studies also showed that existing adaptation practices were insufficient in offsetting heat stress on maize in the North China Plain[9,58]. Region II would suffer compound water-heat stress even with dynamic adaptation under 2050s and 2080s because of severe individual water and heat stresses projected by all GCMs under all planting dates with different cultivars under both scenarios (Supplementary Figs. 18–21). Furthermore, the adaptation capacity was projected to decrease over time in most regions, except for region III (Supplementary Fig. 9). This was attributed to substantial increases in WHSI over time period in most regions, whereas WHSI exhibited insignificant change in region III (Fig. 3c). Our findings suggest that the increase in WHSI in the future could not be offset by adjusting planting dates and cultivar maturity types. Therefore, additional efforts are needed to mitigate heat stress, such as developing more heat-tolerant cultivars and using biological and chemical agents[39,59].

Although our study revealed the spatiotemporal change of compound water-heat stress and explored the possible adaptation strategies to compound stress, some limitations still require further attention. One key limitation is that the adaptation strategies considered in this study are restricted to adjustments in planting date and cultivar maturity, reflecting a focus on cost-effective and readily implementable options for farmers. Other strategies, such as irrigation and improved cultivars with drought and heat tolerance, were not included and may further enhance adaptation potential, while also introducing additional uncertainties related to water availability and management practices. Moreover, we focused on adaptation to mitigate compound stress around maize flowering. However, maize yield is determined by the meteorological factors during the entire growth period. Therefore, adaptation options that consider only compound stress around maize flowering may lead to unfavorable growth conditions during other growth stages (e.g., late frost events and precipitation deficits due to shifted growing seasons). We found that the use of early-maturing cultivars may avoid compound stress in most maize planting regions, but late-maturing cultivars may have higher yields under conditions without severe compound stress[7]. Therefore, it merits further follow-up studies that evaluate adaptation options considering climatic conditions during the whole growth period and the length of the growing period[60]. Finally, this study does not explicitly account for economic costs, feasibility, and other interacting factors such as pest pressures and farmer adoption constraints, which may influence the effectiveness of adaptation strategies in real-world systems. Integrating economic evaluation and broader system interactions with biophysical modeling would provide a more comprehensive assessment and represents an important direction for future research.

The combination of water and heat stresses has the potential to inflict substantial harm on agriculture, society, and the economy[61]. Our research represents a great stride in evaluating the occurrence and severity of such compound stress for maize, and quantifying the potential of multiple adaptation strategies to reduce the risk of compound events. With further advances in understanding the impacts of compound water-heat stress on crop yields, the compound stress index could be continuously improved to evaluate its impact on crop yield together with improved crop models[62,63], thereby safeguarding future global food security. The framework developed here can readily be expanded to encompass different geographic areas and crops, facilitating the development of effective targeted adaptation measures. However, its application to other systems requires appropriate calibration of crop-specific parameters, stress thresholds, and phenological stages, as well as consideration of local climate regimes and management practices. This highlights the potential for broader application of the WHSI framework in supporting climate risk assessment and adaptation planning under diverse agro-climatic conditions.

Methods

Study area, soil, and climate data

We selected 277 meteorological sites within a 30 km distance to China's maize planting area, where the percentage of maize planting area was above 5% of each grid (Supplementary Fig. 4a). The delineation of China's maize planting area with a resolution of 0.1° × 0.1° was obtained from the Spatial Production Allocation Model (SPAM2010)[64]. We divided China's maize growing area into five regions based on geographic locations and cropping systems (Supplementary Table 11). Soil data for physical and chemical properties, including bulk density, saturated water content, field capacity, and wilting point, were obtained from the Global High-Resolution Soil Profile Database (http://soilgrids.org) (Supplementary Note 4).

Daily climate data of each site were statistically downscaled from gridded monthly climate data based on 22 Global Climate Models (GCMs) from CMIP6[9,65], including solar radiation (MJ m^{-2} d^{-1}), precipitation (mm), maximum and minimum air temperatures (°C). Specifically, the gridded monthly climate data were downscaled to the site level using the spatial inverse distance-weighted (IDW) interpolation method. Then, biases of monthly data at each site were corrected by comparing projected and observed data during the historical training period in 1985–2016[9]. Daily data were subsequently produced from the bias-corrected monthly data using a stochastic weather generator[65]. To assess the impact of climate

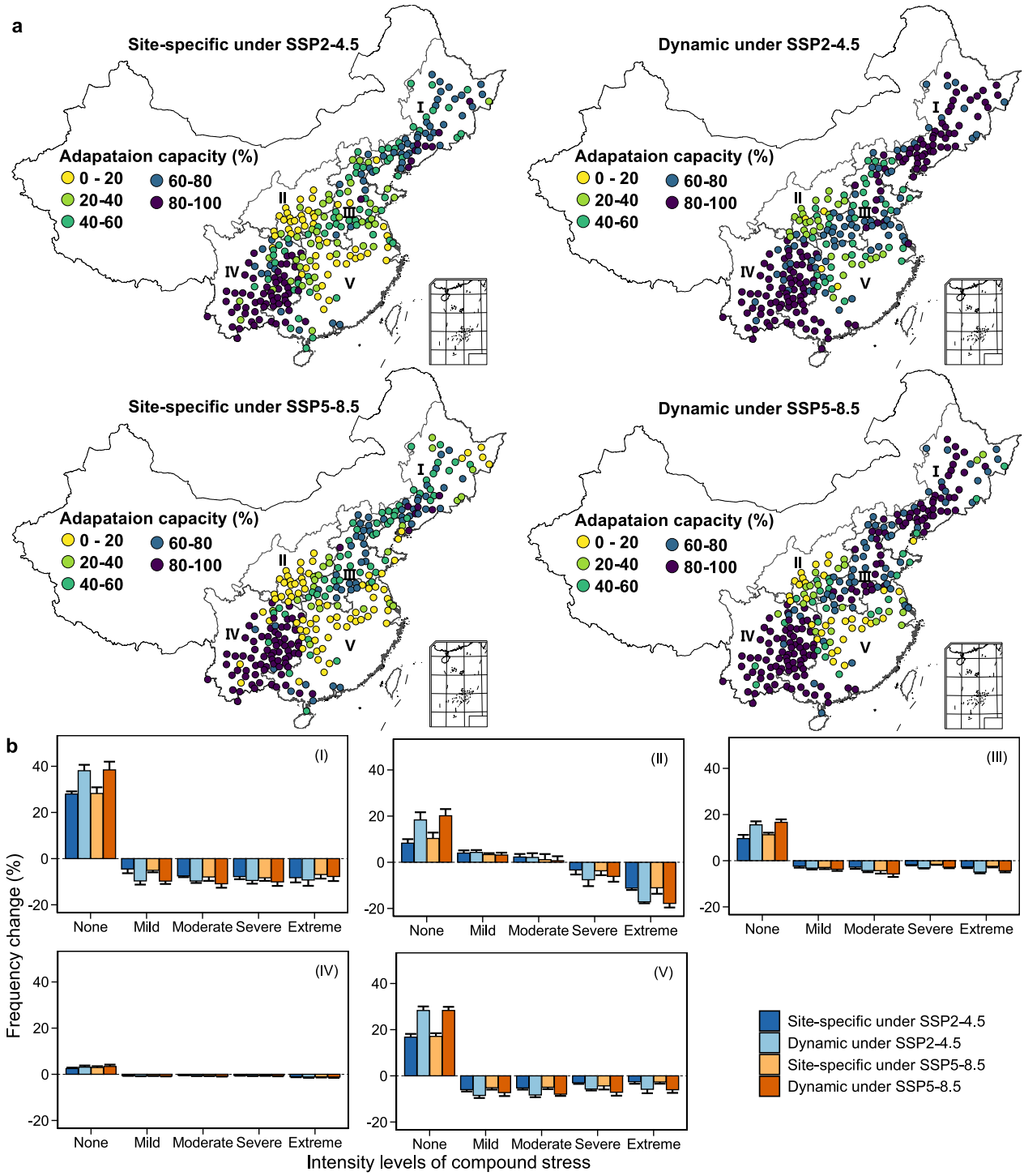


Fig. 6 | The capacity of different adaptation levels to compound water-heat stress in China's Maize Belt. a The distribution of adaptation capacity of site-specific adaptation and dynamic adaptation averaged from 1980 to 2099 under SSP2–4.5 and SSP5–8.5, respectively. **b** Changes in the frequency of different levels of compound stress with and without adaptation options. Bars represent the mean projected adaptation capacity across GCMs under both scenarios for 1980–2099, and error bars represent the SD of five GCMs. The definitions of regions I–V are the same as in Fig. 3.

change on maize, we divided 22 GCMs under SSP5–8.5 and SSP2–4.5 into five representative climate subsets by precipitation and temperature changes, respectively (Supplementary Fig. 4b, c). Then we selected five GCMs from representative climate subsets in China's Maize Belt (relatively hot/wet, hot/dry, middle, cold/wet, and cold/dry) (Supplementary Note 5, Supplementary Table 4), capturing the profile of change in precipitation and temperature for all GCMs ensemble[66]. The study period was divided into four periods, i.e., the baseline (1980–2009), 2020s (2010–2039), 2050s (2040–2069), and 2080s (2070–2099). Supplementary Figure 22 shows the framework of this study.

Simulation of maize phenology and water balance by APSIM

In this study, the APSIM model with well-calibrated crop genotype parameters was used to simulate the phenology and evapotranspiration (ET) of maize. The APSIM model has been used in a large number of studies on the impacts of climate change on maize growth and development worldwide[7,67].

To determine the genetic parameters specific to different maize cultivars, we compared observed data of phenology and yield with simulated data from the APSIM model, ensuring a robust and accurate representation of maize performance[7] (RMSE < 2.7 d for flowering stage and NRMSE < 20% for yield; Supplementary Fig. 23, Supplementary Table 12).

In the simulation, planting dates (Supplementary Fig. 24), cultivars (Supplementary Table 13), and agronomic management practices were set based on the records from 212 agro-meteorological sites in China's maize planting regions (Supplementary Note 6, Supplementary Fig. 4a). Maize was planted under rainfed conditions with a planting density of 67,500 plants ha^{-1}, without any nitrogen limitations. The initial soil water content in the top 150 cm soil depth was set as 30% of the plant available water holding capacity for regions I and III, and 81% for regions IV and V, taking into account the local precipitation conditions in each respective region[9].

Water stress index, heat stress index, and compound water-heat stress index

Both water and heat stresses can damage maize growth and yield formation, particularly when these stresses occur around flowering of maize, hereafter referred to as "growth critical period"[68,69]. Therefore, we focused on the impact of compound water-heat stress during the critical period of 10 days before to 20 days after the flowering date, covering a total of 31 days, including the processes of silking, pollination, and early grain filling[69,70]. To consider the impact of soil water dynamics on maize, the APSIM model was used to simulate soil water content, potential, and actual evapotranspiration during the maize growing period.

We utilized the water stress index (WSI) and the Heat Stress Index (HSI) to assess the occurrence and intensity of water and heat stresses during the flowering period of maize. Following the methodology described in the study by Couëdel et al.[71], we computed the WSI using the equation:

$$WSI = \sum_{i=1}^{n}(1 - ET_a/ET_p)/n \tag{1}$$

where i represents a specific day during the flowering period (10 days before to 20 days after the flowering date), n represents the duration of flowering period, i.e., 31 days. ET_a and ET_p are the daily actual and potential evapotranspiration (mm), respectively.

HSI was calculated as follows[72]:

$$HSI_d = \begin{cases} 0 & for T_{\max} < T_{opt} \\ \frac{T_{\max} - T_{opt}}{T_c - T_{opt}} & for T_{opt} \le T_{\max} < T_c \\ 1 & for T_{\max} \ge T_c \end{cases} \tag{2}$$

$$HSI = \sum_{i=1}^{n} HSI_d/n \tag{3}$$

where HSI_d is the daily heat stress index, T_{max} is the daily maximum air temperature, and T_{opt} and T_c are optimum temperature and ceiling temperature respectively for maize growth during the flowering period. During the critical period, T_{opt} and T_c are set to 29 and 39 °C for the pre-anthesis stage, 30 and 37 °C for the anthesis stage, and 27 and 36 °C for the early grain-filling stage, respectively[33]. To evaluate the effectiveness of the HSI in capturing heat stress impacts, we compared its performance with the default APSIM-simulated yield loss rate. The HSI showed consistently stronger correlations with observed de-trended maize yields across provinces, indicating an improved ability to capture yield losses associated with heat stress (Supplementary Fig. 25).

Therefore, the values of WSI and HSI reflect the frequency and intensity of water and heat stress events during the maize flowering period, respectively. The WSI and HSI range from 0 to 1. Both indices are harmful above 0 as the soil water becomes deficient for maize growth or the temperature exceeds the threshold for maize flowering. The larger values of WSI and HSI represent the more harmful stress.

Compound water-heat stress was defined in this study as the joint occurrence of water and heat stresses over at least three consecutive days[61]. We developed an index called the Water-Heat Stress Index (WHSI) to characterize the frequency and intensity of compound water-heat stress.

A joint cumulative probability was applied to express the compound water-heat stress, which has been commonly used in assessing the intensity of combined events[73]. In this study, we defined compound stress as the two interdependent variables X (WSI) and Y (HSI) in all samples, both of which exceeded their respective thresholds x and y. The values of threshold x (WSI) and y (HSI) are the specific values for which we aim to calculate the joint cumulative probability. The WHSI was developed with a bivariate copula function c based on interdependence between WSI and HSI to generate a bivariate distribution linking these two indices[20]. The copula function proposed by Sklar[74] is a mathematical function that connects multivariate distributions to their marginal distribution, which has been widely used to calculate joint probability distribution between dependent variables[20,73]. The joint cumulative probability p of compound stress was calculated as:

$$\begin{aligned} p =& P(X > x,\ Y > y) = 1 - P(X \le x) - P(Y \le y) + P(X \le x, Y \le y) \\ &= 1 - u - v + c(u, v) \end{aligned} \tag{4}$$

where u and v are uniform marginal distributions transforming from X and Y. $c(u,v)$ is the bivariate joint probability distribution derived from combination of marginal distribution and fitted copula. The copula parameters were estimated using maximum pseudo-likelihood estimation (MPL), as implemented in the R package *VineCopula*.

To determine the most suitable bivariate copula for modeling the joint probability distribution, we evaluated several commonly used copula families, including Gaussian (normal), Gumbel, Clayton, and Frank copulas. The selection process was conducted using the R package *VineCopula*. Model performance was evaluated based on the Akaike Information Criterion (AIC), and the copula with the lowest AIC value was selected. The Gaussian (normal) copula was identified as the best-performing model for China's maize planting regions.

In order to facilitate the comparison of compound stress levels across different sites, we transformed the joint cumulative probability, denoted as p, into an indicator. For intuitive understanding, we calculated the index as $1 - p$ so that the higher values mean more severe stress. Referencing the standardization procedure for calculating the extreme index[75], above $1 - p$ was converted into the water-heat stress index (WHSI). Specifically, the exceedance probability $(1 - p)$ was transformed into a uniform distribution by empirical cumulative distribution function F, and then standardized using the inverse standard normal distribution φ^{-1} to obtain a comparable index. The calculation of WHSI is as follows:

$$WHSI = \varphi^{-1}(F(1 - P(X > x,\ Y > y))) \tag{5}$$

The levels of compound water and heat stresses

To clarify severity of climate change impacts on compound stress intensities, we classified it into four levels based on the WHSI across all sites, years and GCMs (Fig. 3b). The thresholds for each level of compound stress were determined using cumulative probability: extreme (cumulative probability ≥ 75%), severe (75% > cumulative probability ≥ 50%), moderate (50% > cumulative probability ≥ 25%), and mild (25% > cumulative probability > 0). To ensure comparability across regions, the same WHSI thresholds were applied uniformly across all sites, years, and GCMs. The corresponding WHSI values for extreme, severe, moderate, and mild compound stress are above 0.8, between −0.4 and 0.8, between −1.1 and −0.4, and below −1.1, respectively.

The occurrence frequency of compound stress at all levels was calculated to assess its severity at each site.

$$f(\%) = m/M \times 100 \quad (6)$$

where f represents the occurrence frequency of compound stress at different levels (none, mild, moderate, severe, and extreme). m is the number of years corresponding to each level of compound stress, and M is the total number of years (e.g., 30 years).

To evaluate the impact of adaptation, the change in frequency of compound stress at all levels was calculated, identifying which levels could be reduced through adaptation.

$$f_c = f_{wa} - f_a \quad (7)$$

where f_c is the frequency change due to adaptation, f_{wa} is the frequency of compound stress at all levels without adaptation, and f_a is the frequency with adaptation.

Multi-level adaptation framework

In this study, we shifted flowering dates by adjusting the combination of planting dates and cultivar maturity types to alleviate the co-occurrence of water and heat stresses during the critical period. The adjustment of planting dates was carried out within the potential planting window, with intervals of 3 days for region III and 7 days for other regions due to a shorter planting window in region III. For single cropping system regions (I–II), the beginning date of the planting window was determined as the day when the 5-day moving average of the daily average temperature exceeded 8 °C (Supplementary Fig. 26). In multiple cropping system regions (III–V), the beginning date of the planting window was defined as the planting date recorded by agro-meteorological sites. We utilized a total of 11 serial planting dates to adjust planting dates in each region, with the 11th planting date representing the end date of the planting window. Apart from reaching physical maturity, maize would be harvested on the day before the first frost day, which is calculated as the day when the daily minimum temperature falls below 0 °C, for regions I–II with the single-cropping system. For regions III–V with the double-cropping system, maize would be harvested three days before planting the next season's crop. To encompass a range of maturity types, maize cultivars were selected, including early-, medium-, and late-maturing cultivars. Three cultivars with different maturities from existing cultivars were selected as representatives in each region (Supplementary Table 14). In total, there are 33 adaptation options for each site to adapt to compound stress.

Two adaptation levels, including site-specific adaptation and dynamic adaptation (Fig. 5), were investigated in this study. The site-specific adaptation considered climate change but without considering interannual climate variability, representing a feasible adaptation option in the current scientific and technological level, and the dynamic adaptation considered climate change and interannual climate variability simultaneously, representing an ideal adaptation option achievable with future scientific and technological advancements. The two adaptation levels were defined as follows:

1) Site-specific adaptation: A specific optimal adaptation strategy was applied at each individual site in each time period. This means that the optimal adaptation strategy varied across sites but remained constant for each site over time. The same adaptation strategy was used to mitigate compound stress at each site throughout the study period.
2) Dynamic adaptation: A specific optimal adaptation strategy was applied at each site and for each year. This means that the optimal adaptation strategy varied both across sites and over time. The adaptation strategy was tailored to each site and adjusted annually to address the changing conditions.

We calculated the adaptation capacity (AC) by quantifying the WHSI change before and after adaptation as follows:

$$\mathrm{AC}(\%) = \frac{\mathrm{WHSI_{wa}} - \mathrm{WHSI_a}}{\mathrm{WHSI_{wa}} - \mathrm{WHSI_{non}}} \times 100 \quad (8)$$

where $\mathrm{WHSI_{wa}}$ represents the compound stress index without adaptation, WHSI_a represents the compound stress index with adaptation and $\mathrm{WHSI_{non}}$ is the WHSI with the non-compound stress taking the value of −3.1 in our study.

Reporting summary

Further information on research design is available in the Nature Portfolio Reporting Summary linked to this article.

Data availability

Meteorological data, soil data, and maize yield datasets used for the construction, validation, and trend analysis of the compound water–heat stress index (WHSI) are publicly available through Zenodo at https://doi.org/10.5281/zenodo.20628172. The datasets generated in this study, including the WHSI, adaptation capacity, and frequency-change datasets used in the analyses, are publicly available through Zenodo at https://doi.org/10.5281/zenodo.20482699. Together, these repositories contain the minimum datasets required to reproduce the analyses and figures presented in this study and to interpret, replicate, and build upon the findings reported in this article.

Code availability

The main code used for data analysis and figure generation in this study is publicly available at https://doi.org/10.5281/zenodo.20482790.

Received: 8 August 2025; Accepted: 25 June 2026;
Published online: 06 July 2026

References

1. Gaupp, F., Hall, J., Hochrainer-Stigler, S. & Dadson, S. Changing risks of simultaneous global breadbasket failure. *Nat. Clim. Change* **10**, 54–57 (2019).
2. Bren d'Amour, C. et al. Future urban land expansion and implications for global croplands. *Proc. Natl. Acad. Sci. USA* **114**, 8939–8944 (2017).
3. UN_DESA. United Nations, Department of Economic and Social Affairs, Population Division. World population prospects: The 2017 revision, key findings and advance tables. ESA/P/WP/248. Retrieved from https://population.un.org/wpp/DataQuery (2017).
4. van Vliet, J., Eitelberg, D. A. & Verburg, P. H. A global analysis of land take in cropland areas and production displacement from urbanization. *Global Environ. Chang.* **43**, 107–115 (2017).
5. IPCC. Summary for Policymakers. In (eds V. Masson-Delmotte et al), *Climate change 2021: The Physical Science Basis. Contribution of Working Group I to the Sixth Assessment Report of the Intergovernmental Panel on Climate Change*. (Cambridge University Press, Cambridge, United Kingdom and New York, NY, USA, 2021), 3949 pp.
6. Jonas, J. et al. Climate impacts on global agriculture emerge earlier in new generation of climate and crop models. *Nat. Food* **2**, 873–885 (2021).
7. Huang, M. et al. Optimizing sowing window and cultivar choice can boost China's maize yield under 1.5 °C and 2 °C global warming. *Environ. Res. Lett.* **15**, 024015 (2020).
8. FAO. Food and Agriculture Organization of the United Nations, Statistics Division. FAOSTAT. Last Updated: June 2025 (2025).
9. Huang, M. et al. Assessing maize potential to mitigate the adverse effects of future rising temperature and heat stress in China. *Agric. For. Meteorol.* **311**, 108673 (2021).

10. Duan, R. et al. Ensemble temperature and precipitation projection for multi-factorial interactive effects of GCMs and SSPs: application to China. *Front. Environ. Sci.* **9**, 742326 (2021).
11. Zhang, C. et al. Characteristics of dry-wet climate change in China during the past 60 years and its trends projection. *Atmosphere* **13**, 275 (2022).
12. Kang, S. & Eltahir, E. A. B. North China Plain threatened by deadly heatwaves due to climate change and irrigation. *Nat. Commun.* **9**, 2894 (2018).
13. Li, X. et al. Risk analysis of maize yield losses in mainland China at the county level. *Sci. Rep.* **10**, 10684 (2020).
14. Schauberger, B. et al. Consistent negative response of US crops to high temperatures in observations and crop models. *Nat. Commun.* **8**, 13931 (2017).
15. Yu, Y., Tao, H., Yao, H. & Zhao, C. Assessment of the effect of plastic mulching on soil respiration in the arid agricultural region of China under future climate scenarios. *Agric. For. Meteorol.* **256–257**, 1–9 (2018).
16. Geirinhas, J. L. et al. Recent increasing frequency of compound summer drought and heatwaves in Southeast Brazil. *Environ. Res. Lett.* **16**, 034036 (2021).
17. Lesk, C. et al. Stronger temperature–moisture couplings exacerbate the impact of climate warming on global crop yields. *Nat. Food* **2**, 683–691 (2021).
18. Heinicke, S., Frieler, K., Jägermeyr, J. & Mengel, M. Global gridded crop models underestimate yield responses to droughts and heatwaves. *Environ. Res. Lett.* **17**, 044026 (2022).
19. Yin, J. et al. Future socio-ecosystem productivity threatened by compound drought–heatwave events. *Nat. Sustain.* **6**, 259–272 (2023).
20. Zscheischler, J. & Seneviratne, S. I. Dependence of drivers affects risks associated with compound events. *Sci. Adv.* **3**, 1–10 (2017).
21. van der Velde, M., Wriedt, G. & Bouraoui, F. Estimating irrigation use and effects on maize yield during the 2003 heatwave in France. *Agric. Ecosyst. Environ.* **135**, 90–97 (2010).
22. Webber, H. et al. Diverging importance of drought stress for maize and winter wheat in Europe. *Nat. Commun.* **9**, 4249 (2018).
23. Mukherjee, S. & Mishra, A. K. Increase in compound drought and heatwaves in a warming world. *Geophys. Res. Lett.* **48**, e2020GL2009 (2021).
24. Cook, B. I. et al. Twenty-first century drought projections in the CMIP6 forcing scenarios. *Earth's Future* **8**, e2019EF001461 (2020).
25. Lesk, C. et al. Compound heat and moisture extreme impacts on global crop yields under climate change. *Nat. Rev. Earth Environ.* **3**, 872–889 (2022).
26. Wu, X. et al. Projected increase in compound dry and hot events over global land areas. *Int. J. Climatol.* **41**, 393–403 (2020).
27. Manning, C. et al. Increased probability of compound long-duration dry and hot events in Europe during summer (1950–2013). *Environ. Res. Lett.* **14**, 094006 (2019).
28. Hao, Z. et al. A monitoring and prediction system for compound dry and hot events. *Environ. Res. Lett.* **14**, 114034 (2019).
29. Wu, X. et al. Dry-hot magnitude index: a joint indicator for compound event analysis. *Environ. Res. Lett.* **14**, 064017 (2019).
30. Keating, B. A. & Thorburn, P. J. Modelling crops and cropping systems—evolving purpose, practice and prospects. *Eur. J. Agron.* **100**, 163–176 (2018).
31. Wang, N. et al. Modelling maize phenology, biomass growth and yield under contrasting temperature conditions. *Agric. For. Meteorol.* **250-251**, 319–329 (2018).
32. Zhu, P. et al. Dissecting the nonlinear response of maize yield to high temperature stress with model-data integration. *Glob. Chang. Biol.* **25**, 2470–2484 (2019).
33. Sanchez, B., Rasmussen, A. & Porter, J. R. Temperatures and the growth and development of maize and rice: a review. *Glob. Chang. Biol.* **20**, 408–417 (2014).
34. Lizaso, J. I. et al. Impact of high temperatures in maize: phenology and yield components. *Field Crops Res.* **216**, 129–140 (2018).
35. Ben-Ari, T. et al. Identifying indicators for extreme wheat and maize yield losses. *Agric. For. Meteorol.* **220**, 130–140 (2016).
36. Yu, C. et al. Assessing the impacts of extreme agricultural droughts in China under climate and socioeconomic changes. *Earth's Future* **6**, 689–703 (2018).
37. Baum, M. E., Licht, M. A., Huber, I. & Archontoulis, S. V. Impacts of climate change on the optimum planting date of different maize cultivars in the central US Corn Belt. *Eur. J. Agron.* **119**, 126101 (2020).
38. Rahimi-Moghaddam, S., Kambouzia, J. & Deihimfard, R. Adaptation strategies to lessen negative impact of climate change on grain maize under hot climatic conditions: a model-based assessment. *Agric. For. Meteorol.* **253-254**, 1–14 (2018).
39. Challinor, A. J. et al. Current warming will reduce yields unless maize breeding and seed systems adapt immediately. *Nat. Clim. Change* **6**, 954–958 (2016).
40. Wang, J. et al. Increased yield potential of wheat-maize cropping system in the North China Plain by climate change adaptation. *Clim. Change* **113**, 825–840 (2012).
41. Huang, M. et al. Dominant sources of uncertainty in simulating maize adaptation under future climate scenarios in China. *Agric. Syst.* **199**, 103411 (2022).
42. Ruiz-Ramos, M. et al. Adaptation response surfaces for managing wheat under perturbed climate and CO_2 in a Mediterranean environment. *Agric. Syst.* **159**, 260–274 (2018).
43. Hasegawa, T. et al. Extreme climate events increase risk of global food insecurity and adaptation needs. *Nat. Food* **2**, 587–595 (2021).
44. Zipper, S. C., Qiu, J. & Kucharik, C. J. Drought effects on US maize and soybean production: spatiotemporal patterns and historical changes. *Environ. Res. Lett.* **11**, 094021 (2016).
45. Lesk, C. & Anderson, W. Decadal variability modulates trends in concurrent heat and drought over global croplands. *Environ. Res. Lett.* **16**, 055024 (2021).
46. Li, J. et al. A standardized index for assessing sub-monthly compound dry and hot conditions with application in China. *Hydrol. Earth Syst. Sci.* **25**, 1587–1601 (2021).
47. Zhang, Q. et al. Evolution, severity, and spatial extent of compound drought and heat events in north China based on copula model. *Agric. Water Manag.* **273**, 107918 (2022).
48. Yu, R. & Zhai, P. More frequent and widespread persistent compound drought and heat event observed in China. *Sci. Rep.* **10**, 14576 (2020).
49. Su, B. et al. Insight from CMIP6 SSP-RCP scenarios for future drought characteristics in China. *Atmos. Res.* **250**, 105375 (2021).
50. Minoli, S. et al. Global crop yields can be lifted by timely adaptation of growing periods to climate change. *Nat. Commun.* **13**, 7079 (2022).
51. Woo, D. K., Riley, W. J., Grant, R. F. & Wu, Y. Site-specific field management adaptation is key to feeding the world in the 21st century. *Agric. For. Meteorol.* **327**, 109230 (2022).
52. Feng, P. et al. Increasing dominance of Indian Ocean variability impacts Australian wheat yields. *Nat. Food* **3**, 862–870 (2022).
53. Cheng, M. et al. High-resolution crop yield and water productivity dataset generated using random forest and remote sensing. *Sci. Data* **9**, 641 (2022).
54. Peng, B., Guan, K., Pan, M. & Li, Y. Benefits of seasonal climate prediction and satellite data for forecasting U.S. maize yield. *Geophys. Res. Lett.* **45**, 9662–9671 (2018).
55. Shuai, G. & Basso, B. Subfield maize yield prediction improves when in-season crop water deficit is included in remote sensing imagery-based models. *Remote Sens. Environ.* **272**, 112938 (2022).

56. Monego, V. S., Anochi, J. A. & Velho, H. F.dC. South America seasonal precipitation prediction by gradient-boosting machine-learning approach. *Atmosphere* **13**, 243 (2022).
57. Yin, G., Yoshikane, T., Kaneko, R. & Yoshimura, K. Improving global subseasonal to seasonal precipitation forecasts using a support vector machine-based method. *J. Geophys. Res. Atmos.* **128**, e2023JD038929 (2023).
58. Gao, Z. et al. Adjusting the sowing date of spring maize did not mitigate against heat stress in the North China Plain. *Agric. For. Meteorol.* **298-299**, 108274 (2021).
59. Liu, X. et al. High temperature defense-related pathways, mediating lodicule expansion and spikelet opening in maize tassel. *J. Exp. Bot.* **74**, 3684–3699 (2023).
60. Minoli, S., Egli, D. B., Rolinski, S. & Müller, C. Modelling cropping periods of grain crops at the global scale. *Global Planet. Change* **174**, 35–46 (2019).
61. Yin, J. et al. Global increases in lethal compound heat stress: hydrological drought hazards under climate change. *Geophys. Res. Lett.* **49**, e2022GL100880 (2022).
62. Maiorano, A. et al. Crop model improvement reduces the uncertainty of the response to temperature of multi-model ensembles. *Field Crops Res.* **202**, 5–20 (2017).
63. Sun, T. et al. Current rice models underestimate yield losses from short-term heat stresses. *Glob. Chang. Biol.* **27**, 402–416 (2020).
64. IFPRI. International Food Policy Research Institute, Global Spatially-Disaggregated Crop Production Statistics Data for 2010 Version 2.0, 10.7910/DVN/PRFF8V, Harvard Dataverse, V4. (2019).
65. Liu, D. L. & Zuo, H. Statistical downscaling of daily climate variables for climate change impact assessment over New South Wales, Australia. *Clim. Change* **115**, 629–666 (2012).
66. Ruane, A. C. & McDermid, S. P. Selection of a representative subset of global climate models that captures the profile of regional changes for integrated climate impacts assessment. *Earth Perspect.* **4**, 1–20 (2017).
67. Hunt, J. R. et al. Early sowing systems can boost Australian wheat yields despite recent climate change. *Nat. Clim. Change* **9**, 244–247 (2019).
68. Mueller, S. M., Messina, C. D. & Vyn, T. J. The role of the exponential and linear phases of maize (*Zea mays* L.) ear growth for determination of kernel number and kernel weight. *Eur. J. Agron.* **111**, 125939 (2019).
69. Wang, Y. et al. High temperature sensitivity of kernel formation in different short periods around silking in maize. *Env. Exp. Bot.* **183**, 104343 (2021).
70. Rattalino Edreira, J. I., Budakli Carpici, E., Sammarro, D. & Otegui, M. E. Heat stress effects around flowering on kernel set of temperate and tropical maize hybrids. *Field Crops Res.* **123**, 62–73 (2011).
71. Couëdel, A. et al. Assessing environment types for maize, soybean, and wheat in the United States as determined by spatio-temporal variation in drought and heat stress. *Agric. For. Meteorol.* **307**, 108513 (2021).
72. Teixeira, E. I. et al. Global hot-spots of heat stress on agricultural crops due to climate change. *Agric. For. Meteorol.* **170**, 206–215 (2013).
73. Zhou, S. et al. Land–atmosphere feedbacks exacerbate concurrent soil drought and atmospheric aridity. *Proc. Natl. Acad. Sci. USA.* **116**, 18848–18853 (2019).
74. Nelsen, R. B. *An Introduction to Copulas* (Springer, 2007).
75. Hao, Z., Hao, F., Singh, V. P. & Zhang, X. Changes in the severity of compound drought and hot extremes over global land areas. *Environ. Res. Lett.* **13**, 124022 (2018).

Acknowledgements

We acknowledge the World Climate Research Program, which, through its Working Group on Coupled Modeling, coordinated and promoted CMIP6. We thank the climate modeling groups for producing and making available their model output, the Earth System Grid Federation (ESGF) for archiving the data and providing access, and the multiple funding agencies that support CMIP6 and ESGF.

Author contributions

M.H., J.W., and B.W. designed the study. M.H. carried out the simulation and calculated the result. M.H., J.W., and B.W. conducted the analysis and drafted the paper. D.L.L. provided daily climate data with a statistical downscaling method. K.X. shared the method for calculating joint cumulative probability. C.M., J.J., S.A., H.Y., and B.L. advised on the interpretation of the results and revised the paper.

Funding

This study was supported by the National Natural Science Foundation of China (42375194), the Strategic Priority Research Program of the Chinese Academy of Sciences [XDA28060200], the Youth Innovation Team of China Meteorological Administration (CMA2023QN15), and the 2115 Talent Development Program of China Agricultural University.

Competing interests

The authors declare no competing interests.

Additional information

Supplementary information The online version contains supplementary material available at https://doi.org/10.1038/s43247-026-03785-5.

Correspondence and requests for materials should be addressed to Jing Wang or Bin Wang.

Peer review information *Communications Earth & Environment* thanks Peng Zhu and the other, anonymous, reviewer(s) for their contribution to the peer review of this work. Primary Handling Editors: Mengjie Wang. A peer review file is available

Reprints and permissions information is available at http://www.nature.com/reprints

Publisher's note Springer Nature remains neutral with regard to jurisdictional claims in published maps and institutional affiliations.

Open Access This article is licensed under a Creative Commons Attribution-NonCommercial-NoDerivatives 4.0 International License, which permits any non-commercial use, sharing, distribution and reproduction in any medium or format, as long as you give appropriate credit to the original author(s) and the source, provide a link to the Creative Commons licence, and indicate if you modified the licensed material. You do not have permission under this licence to share adapted material derived from this article or parts of it. The images or other third party material in this article are included in the article's Creative Commons licence, unless indicated otherwise in a credit line to the material. If material is not included in the article's Creative Commons licence and your intended use is not permitted by statutory regulation or exceeds the permitted use, you will need to obtain permission directly from the copyright holder. To view a copy of this licence, visit http://creativecommons.org/licenses/by-nc-nd/4.0/.

© The Author(s) 2026